

Large Faraday rotation of resonant light in a cold atomic cloud

G. Labeyrie, C. Miniatura and R.Kaiser

*Laboratoire Ondes et Désordre, FRE 2302 CNRS
1361 route des Lucioles, F-06560 Valbonne*

October 23, 2018

Abstract

We experimentally studied the Faraday rotation of resonant light in an optically-thick cloud of laser-cooled rubidium atoms. Measurements yield a large Verdet constant in the range of $200000^\circ/\text{T/mm}$ and a maximal polarization rotation of 150° . A complete analysis of the polarization state of the transmitted light was necessary to account for the role of the probe laser's spectrum.

PACS numbers : 33.55.Ad, 32.80.Pj

1 Introduction

During the past two years, we have been theoretically and experimentally investigating coherent backscattering (CBS) of near-resonant light in a sample of cold rubidium atoms [1, 2, 3]. CBS is an interference effect in the multiple scattering regime of propagation inside random media, yielding an enhancement of the backscattered light intensity [4]. This interference is very robust and can be destroyed only by a few mechanisms, including Faraday rotation [5] and dynamical effects [6]. In the particular case of atomic scatterers, we have shown that the existence of an internal Zeeman structure significantly degrades the CBS interference [1, 3]. The breakdown of CBS due to the Faraday effect in classical samples has been recently observed and studied in details [7], in a situation where the scatterers are embedded in a Faraday-active matrix. We are currently exploring the behavior of CBS when a magnetic field is applied to the cold atomic cloud. Since the Faraday effect is expected to be large even at weak applied fields (of the order of $1 \text{ G} = 10^{-4} \text{ T}$), it seems relevant to evaluate its magnitude in the particular regime of near-resonant excitation.

The Faraday effect, i.e. the rotation of polarization experienced by light propagating inside a medium along an applied magnetic field, is a well-known phenomenon [8]. Faraday glass-based optical insulators are widely used in laser experiments to avoid unwanted optical feedback. Due to the presence of well-defined lines (strong resonances), the Faraday effect is potentially strong in

atomic systems, and has been extensively studied in hot vapors [9]. In addition, light can modify the atomic gas as it propagates and induce alignment or orientation via optical pumping, yielding various non-linear effects [10]. However, our experiment is quite insensitive to these effects and the scope of this paper will only be the linear, "standard" Faraday rotation. Even though laser-cooled atomic vapors appear interesting due to suppression of Doppler broadening and collisions, few experiments on cold atoms are, to our knowledge, reported in the literature [11].

In Section 2 we expose a simple formalism to understand the main characteristics of optical activity in an atomic system. This model, adapted to the atomic structure of Rb, will be used in the quantitative analysis of the experimental results. We also briefly recall in this Section the principles of the Stokes analysis of a polarization state. The experimental setup and procedure are described in Section 3. The results are presented in Section 4, and compared to the model.

2 Faraday effect and dichroism

Let us consider a gas of two-level atoms excited by a near-resonant monochromatic light field of frequency ν . The induced electric dipole has a component in phase with the excitation, which corresponds to the real part of the susceptibility of the atomic medium (with a dispersive behavior), and a component in quadrature, which corresponds to the imaginary part of the susceptibility (absorptive behavior). The former thus relates to the refractive index of the gas, while the latter corresponds to the absorption or scattering. At low light intensity $I \ll I_{sat}$ (where $I_{sat} = 1.6 \text{ mW/cm}^2$ is the saturation intensity for Rubidium), the refractive index n of a dilute gas is given by :

$$n(\delta) \simeq 1 - \rho \frac{6\pi}{k^3} \frac{\delta/\Gamma}{1 + 4(\delta/\Gamma)^2} \quad (1)$$

where ρ is the atomic gas density, $k = 2\pi/\lambda$ the light wave number in vacuum, $\delta = \omega - \omega_{at}$ the light detuning, and Γ the natural width ($\Gamma/2\pi = 5.9 \text{ MHz}$ for Rb). On the other hand, the imaginary part of the susceptibility yields the atomic scattering cross-section σ :

$$\sigma(\delta) = \frac{3\lambda^2}{2\pi} \frac{1}{1 + 4(\delta/\Gamma)^2} \quad (2)$$

with the usual Lorentzian line shape. This term will result in an attenuation $\exp(-\rho\sigma L)$ of the incident light as it propagates over a distance L inside the medium ; the quantity $b = \rho\sigma L$ is the optical thickness of the atomic sample. We thus see that the wave will experience both a phase shift and an attenuation as it propagates.

Let us now consider a $J = 0 \rightarrow J' = 1$ transition excited by a linearly polarized light field. A magnetic field \mathbf{B} is applied along the wavector \mathbf{k} , whose

direction is taken as the quantization axis. The magnetic field displaces the resonance frequencies of the excited state Zeeman sublevels of magnetic number $m_e = \pm 1$ by an amount $m_e \mu B$, where $\mu = 1.4$ MHz/G. The incident linearly-polarized light decomposes as the sum of σ^+ and σ^- waves of equal amplitudes, which couple the unshifted ground state to excited state sublevels of magnetic number ± 1 respectively. These waves thus propagate in media with different refractive indices n^+ and n^- and scattering cross-sections σ^+ and σ^- , and experience different phase shifts and attenuations. If, in a first step, we neglect the absorption term, the two transmitted waves recombine in a linearly-polarized wave, rotated by an angle $\theta = \frac{1}{2}(\varphi^+ - \varphi^-) = \frac{\pi}{\lambda}(n^+ - n^-)L$. This is the Faraday rotation angle. At small magnetic field $\mu B/\Gamma \ll 1$, the rotation angle is simply : $\theta \approx b \times \mu B / (\Gamma/2\pi)$. Thus, at small B , the Faraday angle is simply the optical thickness b times the Zeeman shift expressed in units of the natural width Γ (however, the proportionality between θ and b remains valid for arbitrary magnetic field). It should be emphasized that, in atomic vapors, the Faraday effect is very strong compared to that of standard Faraday materials (like Faraday glasses), due to the high sensitivity of atomic energy levels to magnetic field : for a density $\rho = 10^{10} \text{ cm}^{-3}$, the Verdet constant is $40^\circ/G/\text{mm}$ ($4 \times 10^5^\circ/T/\text{mm}$), more than four orders of magnitude above that of typical Faraday glasses. However, for cold atomic gases, the linear increase of rotation angle with magnetic field is restricted to a small field range of a few Gauss (the Zeeman splitting must remain smaller than the natural width), above which the Faraday effect decreases.

Of course, in the regime of near-resonant excitation we are dealing with, one usually can not neglect absorption. The different attenuations for the σ^+ and σ^- components cause a deformation of the transmitted polarization as well as rotation. The polarization thus becomes elliptic with an ellipticity (ratio of small to large axis) determined by the differential absorption between σ^+ and σ^- light. This effect is known as circular dichroism. The angle θ is then the angle between the initial polarization and the large axis of the transmitted ellipse. We will see how the Stokes analysis allows to extract θ and the ellipticity from the measurements.

Although the simple picture developed above gives access to the main mechanisms of optical activity in a an atomic gas, it does not accurately describe the $F = 3 \rightarrow F' = 4$ transition of the D2 line of Rb^{85} used in this experiment. To expand the description to the case of a ground state Zeeman structure, we will make the simplifying assumption that all the transitions between different ground state Zeeman sublevels are independent. We thus neglect optical pumping and coherences. The refractive index for, say, σ^+ light, then writes as

$$n^+(\delta, B) = \sum_{m=-3}^3 p_m c_m^{+2} n_m^+(\delta, B), \text{ where the } p_m \text{ are the ground state sublevels}$$

populations, the c_m^+ the Clebsch-Gordan coefficients for the various σ^+ transitions, and the $n_m^+(\delta, B)$ the refractive indices for the Zeeman-shifted transitions (a transition from a ground state of magnetic number m_g to an excited state m_e is frequency-shifted by $(m_e g_e - m_g g_g) \mu B$, where $g_e = 1/2$ and $g_g = 1/3$

are the Landé factors for the $F = 3 \rightarrow F' = 4$ transition of the D2 line of Rb⁸⁵). We can express in the same way the total scattering cross-section for each circular polarization. In the absence of magnetic field and assuming a uniform population distribution among the ground state sublevels, the total scattering cross-section on resonance is $\sigma(\delta = 0) \simeq 0.43 \times 3\lambda^2/2\pi$, the 0.43 prefactor being the average of the squared Clebsch-Gordan coefficient (or the degeneracy factor of the transition $\frac{1}{3} \frac{(2F'+1)}{(2F+1)}$).

As discussed above, the polarization of the transmitted light can differ from the incident linear polarization. It is thus necessary to fully characterize the polarization state of the transmitted light. This can be done using the Stokes formalism [12]. Four quantities need to be measured : the (linear) component of the transmitted light parallel to the incident polarization ($I_{//}$), the (linear) orthogonal component (I_{\perp}), the (linear) component at 45° (I_{45°), and one of the two circular components (I_{circ}). The sum of the first two is the total intensity s_0 ; the three other Stokes parameters are : $s_1 = I_{//} - I_{\perp} = 2I_{//} - s_0$, $s_2 = 2I_{45^\circ} - s_0$ and $s_3 = 2I_{circ} - s_0$. One can then compute the three quantities which characterize any polarization state :

$$P = \frac{\sqrt{s_1^2 + s_2^2 + s_3^2}}{s_0} \quad (3)$$

$$\sin 2\chi = \frac{s_3}{s_0 P} \quad (4)$$

$$\tan 2\theta = \frac{s_2}{s_1} \quad (5)$$

Here, P is the degree of polarization of the light, i.e. the ratio of the intensities of the polarized component to the unpolarized one (a pure polarization state yields $P = 1$ while $P = 0$ corresponds to totally unpolarized light). Even though we would not *a priori* expect any unpolarized component, we will see that this analysis is indeed necessary in our case. The quantity $e = \tan(\chi)$ is the ellipticity of the polarized component ($e = \pm a/b$, where a and b are the small and large axis of the ellipse respectively and the + or - sign denotes the sense of rotation of the electric field). The Faraday angle θ is the angle between the large axis of the ellipse and the direction of the incident polarization.

3 Description of experiment

3.1 Preparation of cold atoms

The experimental setup, essentially the same as in our coherent backscattering experiment, is described in detail elsewhere [2]. A magneto-optical trap (MOT) is loaded from a dilute Rb⁸⁵ vapor ($P \sim 10^{-8}$ mbar) using six laser beams (diameter 2.8 cm, power 30 mW), two-by-two counter-propagating and tuned to the red of the $F = 3 \rightarrow F' = 4$ of the Rb⁸⁵ D2 line (wavelength $\lambda = 780$ nm). The

applied magnetic field gradient is typically 10 G/cm. During the experiment, the MOT (trapping beams, repumper, and magnetic field gradient) is continuously turned on and off. The "dark" period is short enough (8 ms) so that the cold atoms do not leave the capture volume and are recaptured during the next "bright" period (duration 20 ms).

To characterize the cold atomic cloud, we measure its optical thickness as described in the next subsection. The shape and size of the cloud is recorded in 3D using fluorescence imaging, by illuminating the sample with a laser beam detuned by several Γ . We use a time-of-flight technique to measure the atom's *rms* velocity, typically 10 cm/s. The atomic cloud contains typically 3×10^9 atoms with a quasi-gaussian spatial distribution ~ 5 mm FWHM (on average, the cloud being usually slightly cigar-shaped), yielding a peak density of $\sim 10^{10}$ cm $^{-3}$.

3.2 Optical thickness and transmitted polarization measurements

The laser probe used for transmission measurements lies in the horizontal plane containing 4 of the trapping beams, at an angle of 25°. It is produced by a 50 mW SDL diode laser injected by a Yokogawa DBR diode laser, whose linewidth is 2-3 MHz FWHM as estimated from the beatnote between 2 identical diodes. This laser is passed through a Fabry-Perot cavity (transmission peak FWHM 10 MHz) before being sent through the atomic cloud. Although this filtering does not significantly reduce the linewidth of the laser, it strongly suppresses the spectral components in the wings of the initial lineshape which limit the accuracy of the transmission measurement. The frequency of the probe can be scanned in a controlled way by ± 50 MHz around the $3 \rightarrow 4$ transition of the D2 line. The probe beam diameter is 1-2 mm, and its polarization is linear (vertical). The power in the probe is typically $0.1 \mu W$, yielding a saturation parameter $s = 2 \times 10^{-3}$. It is turned on for 2 ms (yielding a maximum of about 80 photons exchanged per atoms), typically 5 ms after the MOT is switched off. The transmitted beam is detected by a photodiode after a rough spatial mode selection by two diaphragms of diameter 3 mm, distant of 1 m. The optical thickness measurement is performed without applied magnetic field. As we emphasized in [2], simply measuring the on-resonance transmission yields a strongly biased estimate for the optical thickness b , due to the off-resonant components in the probe laser's spectrum. To overcome this problem, one solution is to scan the laser detuning δ and record the transmission line shape. We describe this curve as the convolution product of the transmission line for a purely monochromatic laser $T(\delta) = \exp(-b(\delta))$ with the laser line shape. If the latter is known, one can extract the optical thickness from the transmission data (for instance from the FWHM of the transmission curve). This method is quite accurate for large values of b , where the width of the transmission curve is only weakly dependent on the laser's linewidth. For small values of b , measuring the transmission at $\delta = 0$ is more accurate but still requires some knowledge of the probe laser's spectrum. When working with dense atomic clouds at non-zero detuning, one

should also keep in mind the possible influence of "lensing" effect (focussing or deflection of the transmitted beam), due to the spatially-inhomogeneous refractive index of the sample. In our case, the rather large cloud size (~ 5 mm) and moderate density ($\sim 10^{10} \text{ cm}^{-3}$) yield a large focal length of about 25 m for the cloud, and a small (but still measurable) lensing effect.

Using the measured size of the cloud and assuming a uniform population distribution in the ground state, we can then obtain the peak atomic density and the number of atoms in the sample. The maximal optical thickness measured in our trap is $b = 24$ (yielding a FWHM for the transmission curve $\Delta\delta \sim 6\Gamma$).

As mentioned in Section 2, the Stokes analysis relies on four transmission measurements. To perform the polarization measurement, we insert a polarimeter in the path of the transmitted beam, as shown in fig.1. It consists of a quarter-wave plate (only used for the circular component), a half-wave plate and a glan prism polarizer (fixed). The rejection factor of the polarizer is $\sim 10^{-3}$. The four transmission signals ($I_{//}$, I_{\perp} , I_{45° and I_{circ}) are recorded as a function of the laser detuning. The degree of polarization, ellipticity and rotation angle can then be computed using expressions (3), (4), and (5).

4 Results and discussion

4.1 Role of detuning

Fig.2 shows a typical example of the raw signals obtained in the four polarization channels necessary for the Stokes analysis detailed in Sec.2. The transmitted intensity is recorded as a function of the detuning (expressed in units of Γ) in the parallel (**A**), orthogonal (**B**), 45° (**C**) and circular (**D**) polarization channels. All curves have been scaled by the incident intensity. These data were obtained for a sample of optical thickness $b = 4.6$ and an applied magnetic field $B = 3\text{G}$. We see on curve (**B**) that more than 10% of the incident light is transferred to the orthogonal channel. On curves (**C**) and (**D**), the off-resonant detected intensities are close to 0.5, since the incident linear polarization projection on each of these channels is $1/2$. The transmission curve (**D**), which corresponds to the σ^+ component, presents a minimum shifted towards positive detunings by the Zeeman effect ; the position of the minimum corresponds roughly to the splitting of the $m_g = +3 \rightarrow m_e = +4$ transition (1.4 MHz/G), which has a maximum Clebsch-Gordan coefficient of 1. Curves (**B**) and (**C**) exhibit noticeable asymmetries, which we will discuss later.

From the data of fig.2, we computed the three curves $P(\delta)$ (**A**), $e(\delta)$ (**B**) and $\theta(\delta)$ (**C**) characterizing the polarization state of the transmitted light (fig.3). We note on the curve (**A**) of fig.3 that the degree of polarization P is not always equal to unity, and can be substantially smaller depending on the parameters. This unexpected observation is due to the finite linewidth of our probe beam : light components at different frequencies, initially all linearly polarized, experience different rotations and deformations while passing through the cloud. Because these components have different frequencies, the result of their recom-

bination, when integrated over a time long compared to their beatnote time, is a loss of polarization (for example, two orthogonal linearly-polarized waves of different frequencies and same intensity yield a totally unpolarized light $P = 0$). The result of the recombination of all the spectral components is not straightforward to predict, since each frequency is transmitted with a different intensity, ellipticity and rotation angle. However, if we assume that all the spectral components are mutually incoherent, the total intensity detected in each channel is the sum of the intensities corresponding to all the spectral components. Thus, in order to compare the experimental data with the model, we convolute the transmission curves $I_{//}(\delta)$, $I_{\perp}(\delta)$, $I_{45^\circ}(\delta)$ and $I_{circ}(\delta)$, as calculated with the model of Sec.2, with the power spectrum of the probe laser. We can then compute the curves $P(\delta)$, $e(\delta)$ and $\theta(\delta)$ using expressions (3), (4), and (5). We stress that the influence of the laser's linewidth is quite strong : even for a (lorentzian) linewidth of a tenth of the natural width, for an optical thickness $b = 5$ and a magnetic field $B = 1G$, the loss of polarization is already 32% ($P = 0.68$). This phenomenon also affects the estimates for the ellipticity and the rotation angle, since these quantities reflect mainly the polarization state of the dominant transmitted spectral component. Indeed, if one again considers the example of the superposition of two waves of different frequencies and polarizations (pure states), the results of the Stokes analysis will vary continuously from one polarization state to the other depending on the intensity ratio of the two waves. In the intermediate regime of comparable intensities, the Stokes analysis will not describe adequately any of the two polarizations. It should be noted that this situation differs from the case where the studied light consist of a polarized component plus a depolarized one [12] ; in this case, the Stokes analysis provides the "correct" result (that is, the ellipticity and angle of the polarized component), even for arbitrarily small proportion of polarized light. We experimentally tested the influence of a polychromatic excitation by superimposing to the normal probe beam a weaker one, obtained from the same laser but detuned by 80 MHz with an acousto-optic modulator. The calculated degradation of $P(\delta)$, $e(\delta)$ and $\theta(\delta)$ account well for the experimentally observed behavior.

Fig.3 (B) shows how the ellipticity e of the polarized component of the transmitted light varies with laser detuning. For $\delta > 0$, it is mainly the σ^+ component of the incident light which is absorbed, yielding a mostly σ^- transmitted polarization (negative ellipticity). On resonance ($\delta = 0$) both components are absorbed in the same proportion, an the transmitted polarization is linear ($e = 0$). Since the ellipticity depends on the differential absorption between circular components, it is a direct measurement of the dichroism in the sample. The curve on fig.3 (C) is the Faraday rotation angle computed from expression (5). The on-resonance rotation in this case is about 40° . The solid lines in fig.3 are obtained with our model using the convolution procedure discussed above ; the probe light spectrum is described by the product of a lorentzian laser lineshape (FWHM = 3 MHz) by a lorentzian Fabry-Perot transmission (FWHM = 10 MHz). We account for the observed asymmetry in the experimental curves by introducing a linear variation in the populations of the ground

state sublevels (i.e. a partial orientation of the sample), with maximum variation $\pm 20\%$ between extreme magnetic numbers $m_g = \pm 3$. We have checked some other possible mechanisms for this asymmetry, such as the proximity of the $F = 3 \rightarrow F' = 3$ transition (121 MHz to the red) or optical pumping, but both effects seem to play a small role. The fact that we were also able to invert the asymmetry by varying the orientation of the magnetic field produced by the compensation coils also favors the hypothesis of a partial orientation of the medium. We actually do see some optical pumping effects, manifested by variations of the measured transmission signals with time during the probe pulse (duration 2 ms). The overall effect of optical pumping is to increase the Faraday rotation as the number of exchanged photons (i.e. time) increases, i.e. the measured rotation immediately after turning on the probe is smaller than after 2 ms of presence of the light (by about 6%).

The comparison of fig.3 between experiment and theory shows that, despite some discrepancies due to our rather vague knowledge of the probe lineshape and to the simplicity of our model, the overall agreement is quite satisfying.

4.2 Role of magnetic field

To determine the Verdet constant, it is necessary to measure the Faraday angle as a function of the magnetic field. Fig.4 shows such curves obtained for two different optical thicknesses : $b = 0.75$ (solid circles) and $b = 9$ (open circles). For each curve, the on-resonance Faraday angle θ is scaled by the optical thickness of the cloud, since one expects the rotation to be proportional to the optical thickness (thus, all experimental data should lie on the same "universal" curve). The solid line is the prediction of the model with an infinitely narrow probe laser. Its slope around $B = 0$ is about $10^\circ/G$, yielding a Verdet constant $V = 20^\circ/G/mm$ for an optical thickness $b = 10$ and a sample diameter of 5 mm. The dashed curve represents the small optical thickness limit when the laser linewidth is taken into account, which lowers the slope at around $6^\circ/G$.

Both curves exhibit the expected dispersive shape, with a linear increase of the Faraday angle at small magnetic field values (where the Verdet constant is defined), and then a decreasing rotation when the splitting between the σ^+ and σ^- transitions becomes larger than the natural width. The experimental curve for small optical thickness is quite close to the model prediction (dashed line). For larger values of the optical thickness, the measurements depart from this ideal situation due to the finite linewidth of the laser : the curve for $b = 9$ presents a smaller slope around $B = 0$ and the scaled rotation is globally reduced. As the optical thickness is further increased, the transmitted light becomes increasingly dominated by off-resonant components of the laser spectrum and the information about the central (resonant) frequency is lost. This process is further illustrated in the following subsection.

4.3 Role of optical thickness

In the ideal case of a monochromatic laser, one expects the Faraday rotation to increase linearly with optical thickness. We thus recorded the rotation at $\delta = 0$ and a fixed value of B , as a function of the optical thickness which was varied by detuning the trapping laser. The result of such an experiment is shown in fig.5. The open circles correspond to an applied magnetic field $B = 2$ G, while the solid circles are for $B = 8$ G. The solid line is the expected evolution for $B = 8$ G and a monochromatic laser; the dashed line is the prediction of the same model for $B = 2$ G. We see that, for the higher value of B , the expected linear behavior is indeed obtained, yielding a slope of about $8^\circ/G$. The (absolute) rotation angle increases up to $\sim 150^\circ$. However, the evolution observed at smaller magnetic field ($B = 2$ G, circles) is quite different, where the data quickly depart from the linear evolution even at low optical thickness and suddenly drop towards positive values of the angle at large optical thickness. Qualitatively, this reflects the fact that, at small applied field and large optical thickness, the central (resonant) frequency of the probe laser is strongly attenuated and can become smaller than other (off-resonant) spectral components. The measured rotation angle then passes continuously from the angle of the central frequency component to that of the dominant detuned component (in the wings of the absorption line), which can be negative (see fig.3 (C)). The large dispersion of the data for $B = 2$ G above $b \sim 12$ is due to the important relative error in this low transmission regime. At larger B field, the on-resonance transmission increases due to the Zeeman splitting, and the central frequency component remains dominant for larger values of the optical thickness (for instance, the total transmission at $b = 20$ is around 0.1 for $B = 8$ G, while it is only 3×10^{-3} for $B = 2$ G).

Thus, the simple model of Section 2 provides us with a good description for the various behaviors observed experimentally. A fair quantitative agreement is obtained for moderate optical thickness or high magnetic field. The model is also helpful to understand the important role played by the lineshape of the probe laser in this experimental situation of optically-thick sample and resonant light. The experimental data confirm the occurrence of large Faraday effect inside our atomic cloud, with a Verdet constant in the range of $20^\circ/G/mm$ for a typical optical thickness of 10.

5 Conclusion

We have reported in this paper the measurement of large Faraday effect in an optically-thick sample of cold rubidium atoms. Due to near-resonant excitation, we need to take into account both Faraday rotation (differential refractive index) and dichroism (differential absorption) to analyze the experimental data. Using a very simple model for our $F = 3 \rightarrow F' = 4$ transition, we obtain a good agreement with the experimental data. We measure large Verdet constant of the order of $20^\circ/G/mm$. We have shown that the finite width of the laser spectrum plays a crucial role in the signals obtained for an optically-thick sample.

A complete analysis of the transmitted light polarization state is then necessary to correctly interpret the data.

The determination of the Verdet constant V in the cloud is an important step in our current study of the effect of an applied magnetic field on the coherent backscattering of light by the cold atoms. For Faraday effect to seriously affect the CBS cone, one needs the phase difference between time-reversed waves, accumulated on a distance of the order of the light mean-free path l , to be of the order of π (i.e. a rotation of $\pi/2$ for a linear polarization). This corresponds to a situation where $VBl \sim 1$ [7]. However, the main difference between the situation of ref.[7] (scatterers in a Faraday-active matrix) and our atomic cloud situation is that, in our case, the Verdet constant is determined by the density of scatterers ρ (V proportional to ρ), which in turn fixes the mean-free path (l proportional to $1/\rho$). Thus, *there is a maximum rotation per mean-free path length scale*, which is about 13° (for $B = 3$ G) according to the curve of fig.4 (solid line). It seems to us interesting to study this unusual situation. Our aim is also to understand how the Faraday effect combines to the other effects due to the atom's internal structure to determine the CBS enhancement factor in the presence of an external magnetic field.

Acknowledgement 1 *This research program is supported by the CNRS and the PACA Region. We also thank the GDR PRIMA. The contribution of J.-C. Bernard was determinant in the development of the experiment. We are grateful to D. Delande for some very fruitful discussions.*

6 Bibliography

References

- [1] G. Labeyrie, F. de Tomasi, J.-C. Bernard, C. A. Müller, C. Miniatura & R. Kaiser, *Phys. Rev. Lett.* **83** 5266 (1999).
- [2] G. Labeyrie, C.A. Müller, D.S. Wiersma, Ch. Miniatura and R. Kaiser, *J. Opt. B: Quantum Semiclass. Opt* **2** 672-685(2000).
- [3] T. Jonckheere, C.A. Müller, R. Kaiser, Ch. Miniatura and D. Delande, *Phys. Rev. Lett.* **85**, 4269 (2000).
- [4] M.P. van Albada, A. Lagendijk, *Phys. Rev. Lett.* **55**, 2692 (1985) ; E. Akkermans, P.E. Wolf and R. Maynard, *Phys. Rev. Lett.* **56**, 1471 (1986).
- [5] F.C. MacKintosh and Sajeev John, *Phys. Rev. B* **37**, 1884 (1988); A.S. Martinez and R. Maynard, *Phys. Rev. B* **50**, 3714 (1994); D. Lacoste and B.A. van Tiggelen, *Phys. Rev. B* **61**, 4556 (2000).
- [6] A.A. Golubentsev, *Sov. Phys. JETP* **59**, 26 (1984).
- [7] R. Lenke and G. Maret, *Eur. Phys. J. B* **17**, 171 (2000).

- [8] L.D. Barron, *Molecular Light Scattering and Optical Activity* (Cambridge University Press, Cambridge, 1982).
- [9] F. Schuller, M.J.D. Macpherson, D. N. Stacey, R.B. Warrington and K.P. Zetie, *Optics Comm.* **86**, 123 (1991); M. Kristensen, F.J. Blok, M.A. van Eijkelenborg, G. Nienhuis, and J.P. Woerdman, *Phys. Rev. A* **51**, 1085 (1995).
- [10] G.G. Adonts, D.G. Akopyan, and K. V. Arutunyan, *J. Phys. B : At. Mol. Phys.* **19**, 4113 (1986); W. V. Davis, A.L. Gaeata, and R.W. Boyd, *Opt. Lett.* **17** (18), 1304 (1992); S.I. Kanorsky, A. Weis, J. Wurster, and T.W. Hänsch, *Phys. Rev. A* **47**, 1220 (1993); D. Budker, D.F. Kimball, S.M. Rochester, and V.V. Yashchuk, *Phys. Rev. Lett.* **85**, 2088 (2000).
- [11] T. Isayama, Y. Takahashi, N. Tanaka, K. Ishikawa, and T. Yabuzaki, *Phys. Rev. A* **59**, 4836 (1999).
- [12] Max Born and Emil Wolf in *Principles of Optics*, sixth edition, Pergamon Press, p. 554.

Figures captions:

Figure 1 : Simplified experimental setup.

A probe laser beam of linear polarization \mathbf{E}_i and wave vector \mathbf{k} is sent through the cold atomic cloud, where a magnetic field \mathbf{B} is applied along \mathbf{k} . The polarization \mathbf{E}_t of the transmitted probe light is deformed and rotated. A polarimeter measures the transmitted intensities in four polarization channels : $I_{//}$ (parallel to the incident polarization), I_{\perp} (orthogonal to the incident polarization), I_{45° (at 45° from the incident polarization), I_{circ} (circular polarization). These quantities allow to determine the degree of polarization P , the ellipticity e , and the rotation angle θ of the transmitted light.

Figure 2 : Typical transmission curves in the four polarization channels.

The transmission is measured as a function of the laser detuning (in units of the natural width Γ), for a sample of optical thickness (at zero field) $b = 4.6$ and an applied magnetic field $B = 3$ G. All data are scaled by the total incident light intensity. **A** : intensity $I_{//}$ in the linear parallel channel. **B** : intensity I_{\perp} in the linear orthogonal channel. **C** : intensity I_{45° in the linear 45° channel. **D** : intensity I_{circ} in the circular channel.

Figure 3 : Typical results from the Stokes polarization analysis and comparison with model.

These curves are obtained from the data of fig.2. **A** : degree of polarization P (see expressions (3)). **B** : ellipticity e . **C** : Faraday rotation angle θ . The symbols correspond to experimental data and the solid lines to the predictions of the model described in Sec. II. To reproduce the experimental asymmetry, the model assumes a linear variation of the ground state populations p_m with magnetic number m , with a total variation amplitude of 40% between extreme ground state sublevels $m_g = \pm 3$.

Figure 4 : Scaled Faraday angle as a function of the applied magnetic field B .

The rotation angle θ is scaled by the optical thickness b of the sample. The symbols correspond to samples with two different optical thicknesses : $b = 0.75$ (solid circles) and $b = 9$ (open circles). The solid line is the model prediction assuming a monochromatic probe laser (and a uniform population distribution in the ground state). The dotted line is the small optical thickness limit of the model when taking into account the lineshape of the probe laser.

Figure 5 : On-resonance Faraday rotation angle θ as a function of the optical thickness.

The symbols correspond to experiments with two different values of the magnetic field : $B = 2$ G (open circles) and $B = 8$ G (solid circles). The optical thickness of the atomic cloud is varied by scanning the detuning of the MOT laser. The lines correspond to the predictions of the model with a monochromatic laser, for $B = 2$ G (dashed line) and $B = 8$ G (solid line). For the largest B value, we observe the expected linear increase of Faraday angle with optical thickness. The measured rotation is close to the prediction of the ideal, monochromatic model (solid line). On the other hand, the behavior for $B = 2$ G is quite different : the rotation angle quickly departs from the linear increase, saturates and then decreases. Indeed, as optical thickness increases, the measured rotation becomes increasingly affected by other spectral components of the laser, until these off-resonant frequencies become dominant causing a sharp drop of the angle. At large B the central, resonant frequency component of the laser is always dominant in the optical thickness range investigated, and the linear behavior is recovered.

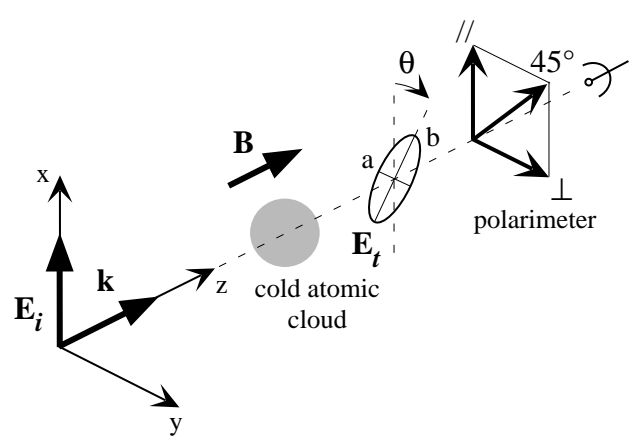


figure 1

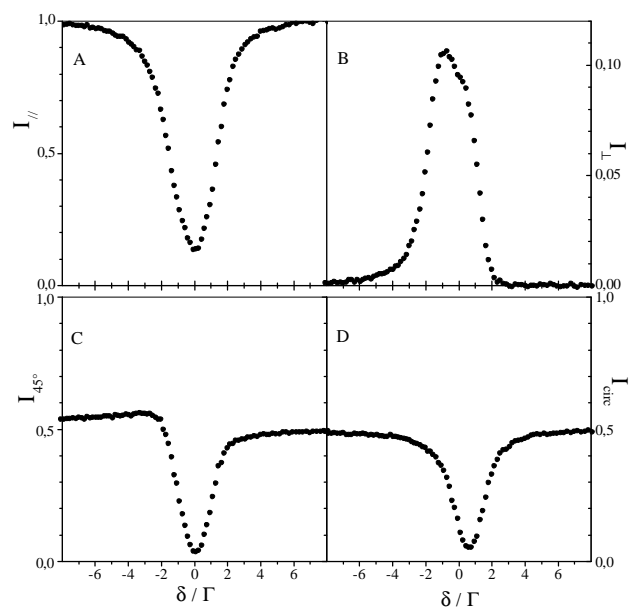
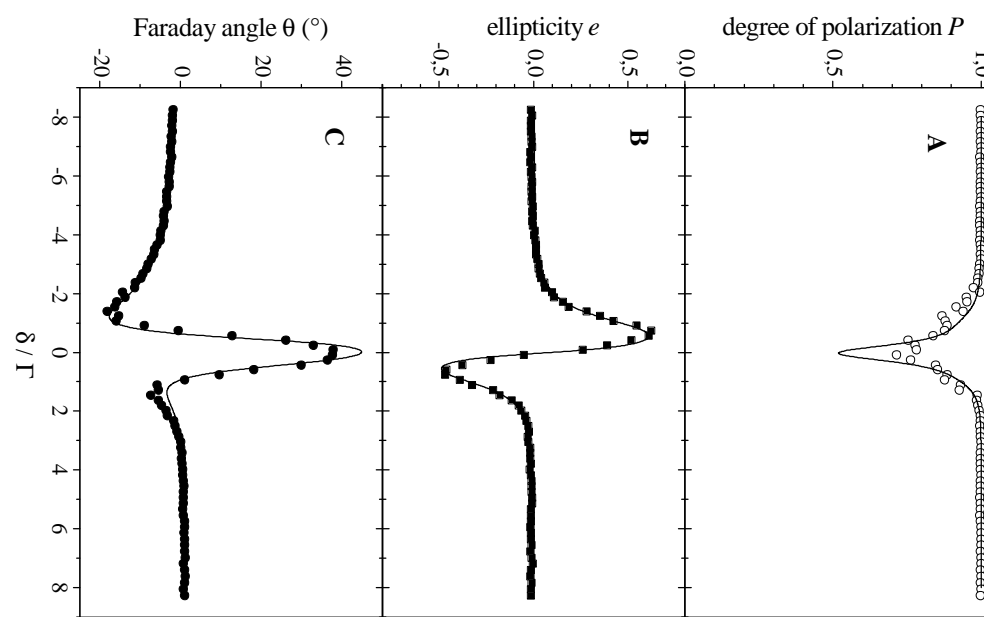


figure 2

figure 3



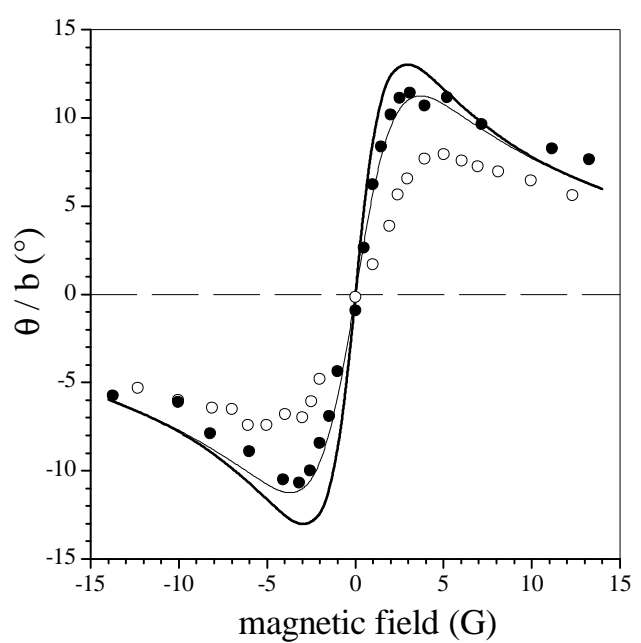


figure 4

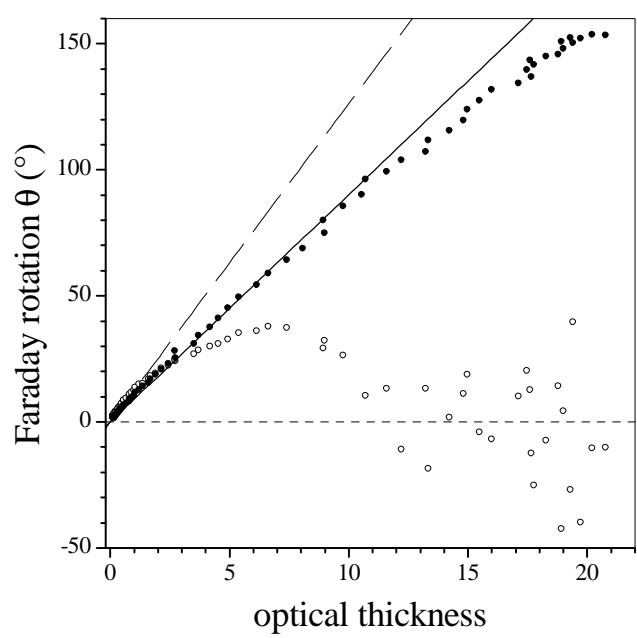


figure 5